PROCEEDINGS, 44th Workshop on Geothermal Reservoir Engineering
Stanford University, Stanford, California, February 11-13, 2019
SGP-TR-214

Investigation of Fracture Permeability Evolution in Phyllite Reservoir Rock Specimen from Blue Mountain Geothermal Field

Bijay K C[1], Arash Kamali-Asl[1], Ehsan Ghazanfari[2], Nicolas Perdrial[3] and Trenton T Cladouhos[4]

[1] PhD Student, Department of Civil and Environmental Engineering, The University of Vermont

[2] Assistant Professor, Department of Civil and Environmental Engineering, The University of Vermont, 33 Colchester Ave., Burlington, VT, 05405

[3] Research Assistant Professor, Department of Geology, The University of Vermont, 180 Colchester Ave., Burlington, VT 05405, USA

[4] Vice-President of Resource, Cyrq Energy, Inc., 4010 Stone Way North, Suite 400, Seattle, WA 98103

Bijay.K-C@uvm.edu; akamalia@uvm.edu; Ehsan.Ghazanfari@uvm.edu; Nicolas.Perdrial@uvm.edu; Trenton.Cladouhos@cyrqenergy.com

Keywords: permeability, fracture aperture, geothermal energy, pressure solution, mechanical creep.

ABSTRACT

Permeability reduction due to mineral dissolution/precipitation in fractured reservoirs is a major concern in geothermal reservoir operations. In order to investigate the evolution of fracture aperture/permeability caused by fluid-fracture surface interactions, a flow-through test was performed on a phyllite specimen retrieved from DB2 well (depth of 1.26 km) at the Blue Mountain geothermal field, Nevada, USA. Permeability evolution of the fractured phyllite specimen was investigated under different states-of-stress (confining pressure and differential pore pressure) at rock temperature of 130 °C and injected geothermal fluid temperature of 65 °C. Fracture aperture/permeability evolution was analyzed using hydraulic data recorded during the course of the experiment. Pre- and post-test X-ray Micro-CT imaging were performed to investigate the flow-induced changes in fracture aperture. Influent and effluent chemistry were analyzed using inductively-coupled plasma optical emission spectrometry (ICP-OES) to determine mineral dissolution during the test. Results indicated a decline in permeability of the specimen due to fracture closure caused by stress corrosion and geo-chemical interactions between the injected geothermal fluid and fracture surface. ICP-OES analyses of the effluent and image analyses indicated that the decrease in fracture aperture was driven by both mechanical and chemical processes.

1. INTRODUCTION

Enhanced Geothermal Systems (EGS), which utilize thermal energy stored in deep bed-rock, has the capacity of producing up to 100 GW of electricity in the United States by 2050 (Tester et al., 2006). A cold water, injected through injection well(s), exchanges heat with the hot bed-rock and a hot water is extracted from the production well(s), which is used for direct heating or for electricity generation via a binary or flash-steam power cycle. The hot dry bed-rocks are generally low permeable. Therefore, hydro-shearing (e.g. Riahi and Damjanac, 2013; Cladouhos et al., 2016), hydraulic fracturing (e.g. Majer et al., 2007; Frash et al. 2014; Oldenburg et al., 2016; Watanabe et al., 2017), or mixed stimulation (e.g. McClure and Horne, 2014) is implemented to enhance permeability of the hot dry bed-rock and hence increase the productivity of an EGS reservoir.

Maintaining permeability of the host bed-rock by keeping the fractures open is key to the long-term success of an EGS. Decrease in permeability of the fracture network leads to decrease in flow rate, production temperature, and hence the electricity generation. Fluid-fracture surface interactions triggered by coupled thermal-hydrological-mechanical-chemical (THMC) processes alter (increase/decrease) the permeability of the fracture network (e.g Taron and Elsworth, 2009; Ghassemi, 2012). THMC processes such as stress-mediated mechanical creep (stress corrosion), chemically-mediated mineral dissolution (and precipitation), and thermally and mechanically activated mineral dissolution (e.g. Polak et al., 2003; Yasuhara et al., 2004; Ghassemi and Kumar, 2007; Faoro et al., 2015) contribute to the evolution of fracture permeability in a long-run. THMC processes in fluid-fracture surface interaction are complex and coupled (e.g. Yasuhara et al., 2004; Taron and Elsworth, 2009). Mechanical effects are active over relatively shorter timescale, while the chemical effects remain active for a prolonged timescale (e.g. Yasuhara et al., 2011).

Several studies have shown that increase in temperature of the injected fluid and rock enhances the dissolution of minerals (e.g. Polak et al., 2003; Yasuhara et al., 2004). Mechanical processes such as increase in effective stress result in crushing of the propping asperities and mechanical creep (e.g. Yasuhara et al., 2011; Vogler et al., 2016). Pressure solution, which incorporates the serial processes of mineral dissolution at contacting asperities, interfacial diffusion, and precipitation at free-faces is a well-known phenomenon that controls the permeability reduction in a fractured rock (e.g. Yasuhara et al., 2004; Yasuhara and Elsworth, 2008). Processes such as reduction in effective stress, dilatant shear, free-face dissolution, and thermal cracking (e.g. Taron and Elsworth, 2009) increase the permeability, whereas processes such as mechanical creep and pressure solution decrease the permeability (e.g. Yasuhara et al., 2011; Caulk et al., 2016; Kamali-Asl et al., 2018).

During the operation phase of an EGS reservoir, stress condition of the host rock changes due to injection/extraction of fluid, fracture stimulation processes, etc. Therefore, it is critical to improve the fundamental understanding of fracture response under different stress

conditions. In this study, results of a flow-through test in a single-fractured phyllite reservoir rock at temperature of 130 °C and injected geothermal fluid temperature of 65 °C under different effective stress conditions (namely, below, at, and above in-situ stress) are presented. The specimen was loaded and unloaded to investigate the reversibility of the fracture aperture/permeability. Results from chemical analysis of the effluent, and pre- and post- test X-Ray micro CT images of the specimen are also presented.

2. MATERIALS

A phyllite core of diameter 2.5 inches, length 9 inches, dry density 2.69 g/cm^3, and a porosity of 0.74% (Figure 1(a)) was retrieved from DB-2 well at a depth of 1260 m adjacent to the Blue Mountain geothermal field located in Nevada, USA (Swyer et al., 2016). As seen in the Figure 1(a), a quartz vein and no apparent micro-cracks were observed in the core. The X-Ray Diffraction (XRD) analysis revealed that the rock was composed of 67.4% quartz, 18.8% albite, 10.5% biotite, and 3.2% chlorite. Effect of material anisotropy was observed on the mechanical response of the core (Kamali-Asl et al., 2019). The permeability of the original core (without any fracture) at close to in-situ condition (i.e. an overburden stress of 30 MPa and a bed-rock temperature of ~ 155 °C) was measured in the lab as ~ 5×10^{-20} m^2. Geothermal fluid extracted from one of the production wells in Blue Mountain geothermal field was used as a working fluid in the study. The fluid had a pH of 7.63 and the concentrations of the dissolved elements in the fluid are presented in the influent column of Table 1 (Section 4.3; Chemical Analysis).

3. EXPERIMENTAL METHODOLOGY

3.1 Sample Preparation

The original core was sub-cored along the direction of the foliation to obtain a rock specimen with a diameter of 38.1 mm and a length of 47 mm. The sub-cored specimen was saw-cut, and the two ends were lapped to 0.001 inches. A single longitudinal fracture along the cylindrical axis (Figure 1(b)) was induced by the modified Brazilian test (Yu et. al, 2009) and exerting tensile stress to the rock specimen.

The fractured specimen was then vacuum-saturated with geothermal fluid. To ensure the full saturation, the specimen was kept submerged in the fluid until the change in the weight between two consecutive days was equal to or less than 0.005 g (scale precision). Then, the two halves of the specimen were well-mated together and inserted inside a Vitton jacket. Finally, the two ends of the specimen were wire-tightened to two core-holders on both ends (Figure 1(c)), and the specimen was placed inside the test vessel (Figures 1(d) and 1(e)).

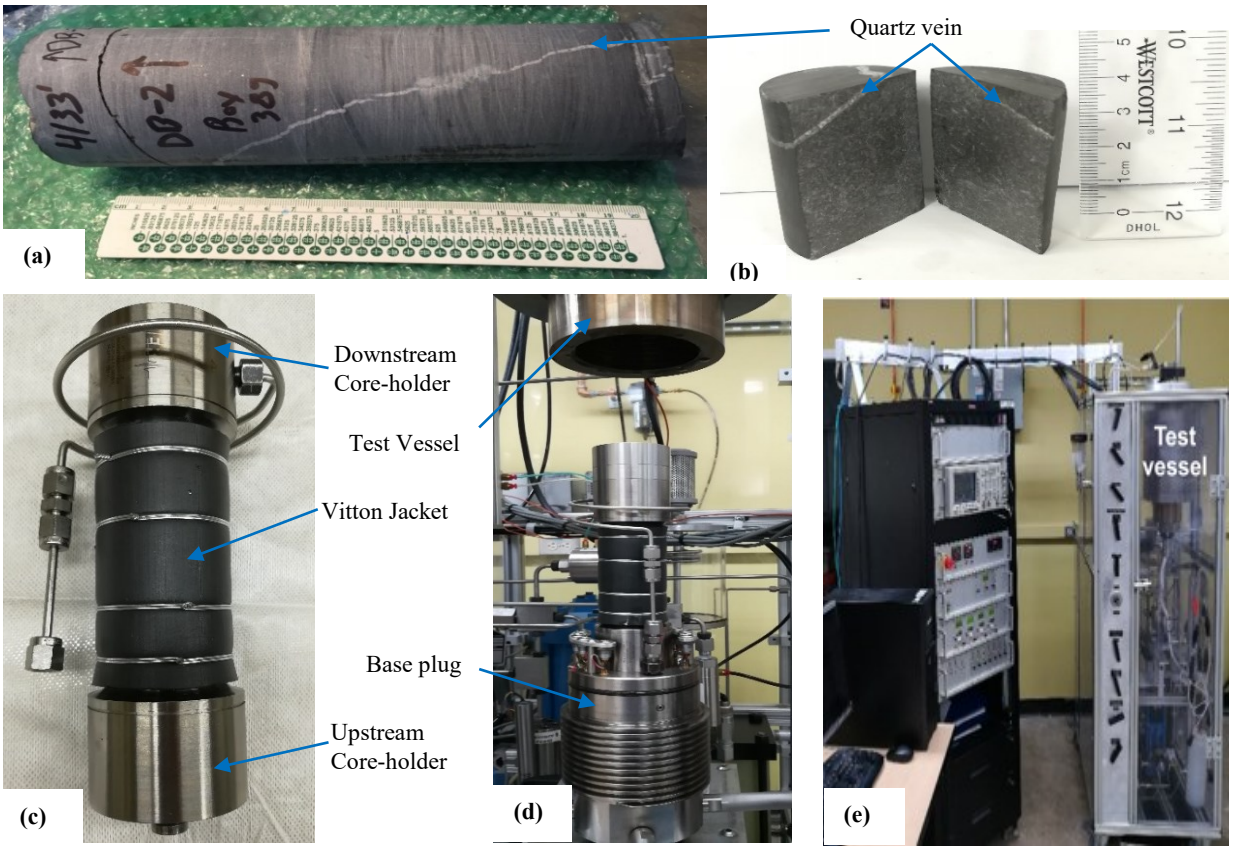

Figure 1: Photo of (a) original core retrieved from the well, (b) fractured specimen, (c) specimen wire-tightened to the core-holders, (d) prepared specimen in base-plug ready to place inside test vessel, and (e) Autolab 1500 instrument.

3.2 Experimental Procedure

A high-pressure/temperature fully servo-controlled triaxial equipment (Autolab 1500) was used to perform flow through test on the fractured phyllite specimen. The instrument is equipped with four separate intensifiers to apply confining pressure (CP) of up to 70 MPa, differential stress (DS) of up to 580 MPa (for specimens having a diameter of 38.1 mm), upstream pore pressure (U/S PP), and downstream pore pressure (D/S PP) of up to 70 MPa. An internal heater inside the test vessel can heat the rock specimen up to the temperature of 130 °C. The working fluid is heated using electrical heaters wrapped around pore pressure tube before being injected into the rock specimen.

Displacement-controlled test (DCT) with a prescribed constant injection rate was performed on the specimen. In DCT, the D/S PP is set at constant value, while the U/S PP intensifier continuously adjusts (i.e. increases or decreases) the U/S PP to maintain the prescribed injection rate. As the flow-induced processes at the fracture surface decreases (or increases) the fracture aperture, the U/S PP increases (or decreases) to maintain the constant injection rate throughout the test. The evolution of differential pore pressure (ΔP = U/S PP – D/S PP) was used as an indicative of the change in fracture aperture.

3.3 Experimental Program

The flow-through experiment was conducted under different stress conditions, i.e. CP of 15 MPa and D/S PP of 5 MPa, CP of 30 MPa and D/S PP of 11 MPa, and CP of 45 MPa and D/S PP of 16 MPa to represent below, at, and above in-situ stress conditions, respectively. Temperature of the rock specimen was maintained at 130 °C, while temperature of the working fluid was maintained at 65 °C throughout the experiment. The injection rate (i.e. flow rate) during the experiment was prescribed at 3.58 ml/day. The injection rate was maintained such that the working fluid have enough residence time to react with the fracture surface and thus, the fracture aperture/permeability evolution due to fluid-fracture surface interaction can be captured. Each stage of the stress condition was held constant for 24 hours before proceeding to the next stress condition. Figure 2 shows the stress path followed during the experiment. Loading and unloading paths were followed during the experiment to investigate the permeability recovery of the specimen.

Before starting the experiment, all the pore pressure tubes were cleaned using alcohol and hot water and vacuum saturated with the geothermal fluid to ensure there is no air in the system prior to flow initialization. The differential pore pressure (i.e. ΔP) measured during the experiment was used to estimate the permeability of the fracture using Darcy's law expressed as:

$$k = \frac{Q\mu L}{A\Delta P} \quad \text{(i)}$$

where, k is permeability (m^2) of the fracture, Q is flow rate through the specimen (m^3/sec), μ is the temperature dependent viscosity of the permeant fluid (Pa.sec), L is length of the specimen (m), A is cross-sectional area of the specimen (m^2), and ΔP is the differential pore pressure (Pa) across the two ends of the specimen.

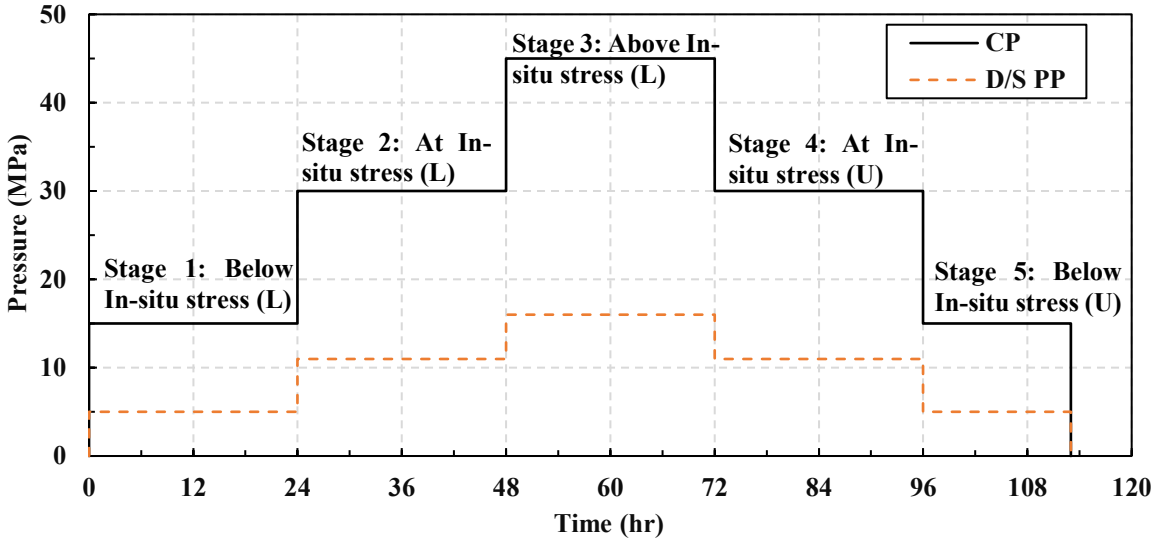

Figure 2: Stress path showing different stress conditions followed during the experiment. L: loading stage and U: unloading stage.

Since the porosity (i.e. 0.74%) and the flow rate (i.e. 3.58 ml/day) were very low, all the flow can be assumed to be contained within the fracture and laminar. Thus, the modified cubic-law with parallel plate approximation was used to estimate the hydraulic aperture of the fracture (e.g. Whiterspoon et al, 1980; Polak et al., 2003, Kamali-Asl et al., 2018), i.e.:

$$b = \left(\frac{12Q\mu L}{d\Delta P}\right)^{1/3} \quad \text{(ii)}$$

where, b is hydraulic aperture (m), and d is the diameter of the specimen (m). Based on the temperature of the injected fluid and the rock specimen, the dynamic viscosity of 3.79×10^{-4} Pa.s was used in above equations to estimate the permeability and hydraulic aperture of the fracture.

After the test was completed, JY Horiba Optima 2 ICP-OES instrument was used to analyze the chemical composition of influent and effluent samples. The samples were diluted by adding 9 g of 1% ultrapure HNO_3 to 1 g of the sample and ICP-OES analysis was performed to detect whether mineral dissolution occurred in the system. A Bruker skyscan 1173 X-Ray micro CT scanner was used to scan the pre- and post-test specimen to investigate the flow-induced changes in fracture aperture of the specimen.

4. RESULTS AND DISCUSSION

4.1 Hydraulic Analysis

The evolution of U/S PP under different effective stresses is shown in Figure 3. During loading stages, a sudden increase in U/S PP was observed while transitioning from lower to higher effective stress, whereas, a sudden decrease in U/S PP was observed during effective stress transitioning in unloading stages. As the effective stress is increased, the two halves of the fractures come closer increasing the contact area at the fracture surface and blocking some flow paths, which cause the U/S PP to increase suddenly in order to maintain the prescribed flow rate. The sudden decrease in the U/S PP during unloading stage is due to stress relaxation which decreased contact area at the fracture surface and opened new flow paths.

During all the stages, U/S PP was gradually increasing indicating the gradual closure of the fractures under all effective stresses. During loading stage, the rates of U/S PP increment were 2.41 Pa/s, 10.83 Pa/s, and 19.03 Pa/s for below, at and over in-situ stress stages, respectively. Moreover, during the unloading stage, the rates of increment were 6.94 Pa/s and 3.36 Pa/s for at and below in-situ stress stages. This observation can be attributed to the fact that at higher effective stresses, the effect of pressure solution and mechanical creep is more pronounced, which leads to higher fracture closure rates (e.g. Faoro et al., 2015; Kamali-Asl et al., 2018).

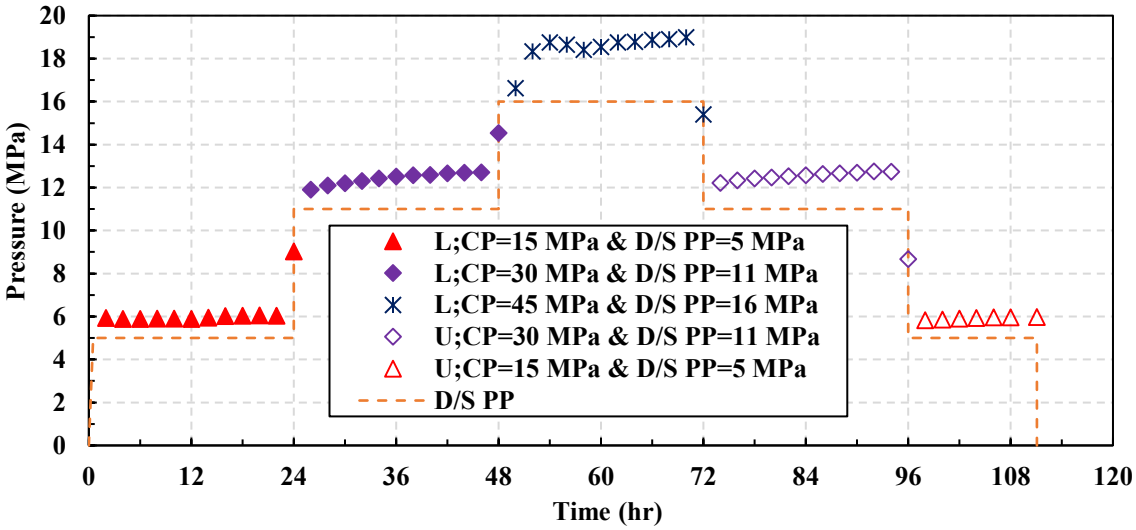

Figure 3: Evolution of upstream pore pressure during different stages of the experiment. L: loading stage and U: unloading stage.

Figure 4 shows the evolution of the fracture permeability and hydraulic aperture under different effective stresses. The permeability and fracture aperture decreased as the effective stress was increased during loading stages, which recovered back during the unloading stages. During the loading stages, the initial sudden increase in the permeability and hydraulic aperture is due to the sudden increase in the downstream pore pressure, which opened the fracture, whereas during the unloading stages, stress relaxation due to a sudden decrease in the confining and downstream pore pressure opened up the fracture. Processes such as pressure solution, mineral dissolution (or precipitation), and mechanical creep can be responsible for the gradual decrease in hydraulic aperture and fracture permeability as observed in this study and several other studies (e.g. Polak et al., 2003; Yasuhara et al., 2004; Caulk et al., 2016; Kamali-Asl et al., 2018). Contribution of mineral dissolution is dominant at lower effective stress and higher temperature, mechanical crushing is dominant at higher effective stress and lower temperature, whereas both mechanisms are active at higher effective stress and higher temperature (e.g. Yasuhara et al., 2011; Faoro et al., 2015)

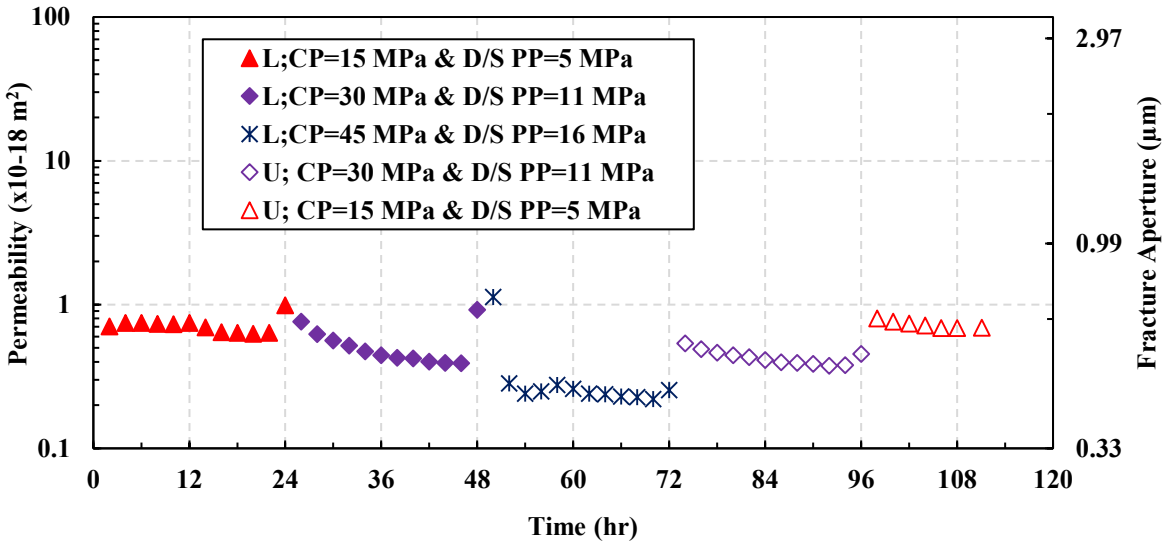

Figure 4: Evolution of permeability and fracture aperture during different stages of the experiment. L: loading stage and U: unloading stage.

4.2 Image Analysis

Figure 5 shows the X-Ray micro CT images of the pre- and post-test specimen at resolution of 24.2 µm. As seen in the figure, the fracture closure is evident in the post-test specimen. As the effective stress was increased during the test, the two fracture surfaces moved close to each other. However, the fracture surfaces did not completely recover their initial positions as the effective stress was decreased. Despite the fracture closure during the test, the U/S pore pressures (Figure 3) and the hydraulic fracture aperture (Figure 4) remained fairly consistent during the loading and unloading stages of same effective stress. This is due to the fact that the channelized flow is the dominant flow type in the fracture. In addition, the pre-and post-test CT images were obtained at atmospheric pressure and room temperature. This prevented estimation of the change in fracture volume along the length of the specimen during the test.

4.3 Chemical Analysis

The results of effluent analysis are summarized in Table 1. Concentration of elements such as Ca, Fe, K, Mg, Na and Si increased in the effluent solution compared to the influent, which indicated the dissolution of rock minerals (Quartz, Albite, Biotite, and chlorite) in the working fluid. The amount of Si that dissolved in the working fluid is low compared to the elements such as Ca, K and Na. This could be due to the fact that minerals (salt) rich in Ca, K and Na are easily dissolvable compared to silicates. Moreover, Si and Al could have formed a complex compound and precipitated in the system (e.g. Caulk et al., 2016; Kamali-Asl et al., 2018). Lower concentration of Mg and Fe in the effluent suggested dissolution of biotite and chlorite was not significant during the test. Since, the effluent chemistry was evaluated at the end of the test, it was difficult to determine the net contribution of mechanical and chemical processes to the permeability evolution of the specimen during each stage of the test.

Table 1: Results of ICP-OES analysis

Elements	Concentration (mg/L)	
	Influent	Effluent
Al	BDL*	BDL
Ca	31.73	80.54
Fe	BDL	0.36
K	92.69	144.14
Mg	BDL	0.22
Na	808.01	1299.71
Si	42.99	56.71

*BDL: Below Detection Limit

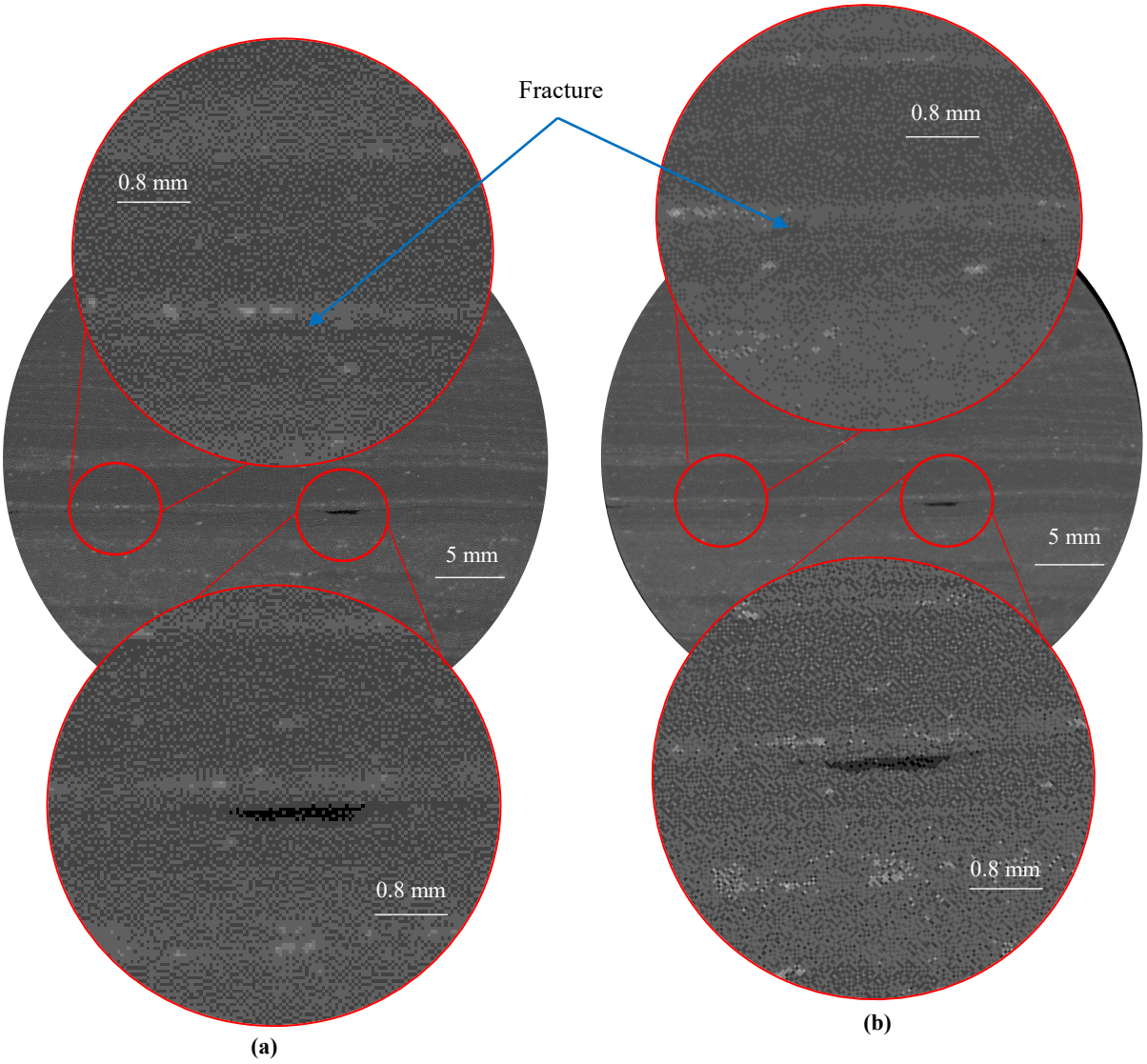

Figure 5: 2D CT image of a cross-section of the specimen (a) pre-test, and (b) post test. The cross-section shown above is at 12 mm from the base of the specimen.

5. CONCLUSION

A flow-through experiment, using geothermal fluid, was conducted on an artificially fractured phyllite specimen at below, at, and above in-situ stress conditions. During the test, temperature of the rock specimen and injected fluid was maintained at 130 °C and 65 °C, respectively. The permeability/hydraulic aperture of the fracture decreased as the effective stress increased due to crushing of the propping asperities, which closed some flow channels, whereas the permeability/hydraulic aperture increased as the effective stress decreased due to stress relaxation. The gradual decrease in the permeability/hydraulic aperture during each stage of the test was due to the combined processes such as pressure solution, mineral dissolution, and mechanical creep, later being dominant under high effective stress. Comparison between pre- and post-test X-Ray CT images showed fracture closure during the test.

Since, the effluent was collected only once at the end of the test, the net contribution of mechanical and chemical processes in the permeability evolution during each stages of the test remained unanswered. Therefore, it is recommended that the effluent be extracted for chemical analysis at the end of each stage to quantify the net effect of each process that results in gradual decrease of the fracture permeability/aperture.

6. ACKNOWLEDGEMENT

The authors would like to thank AltaRock Energy Inc. and University of Nevada, Reno for providing the rock core used in this study. We are also very thankful to National Science Foundation for providing funds for acquisition of the X-Ray micro CT-scanner used in this study. We would also like to thank Mr. Marco vanGemeren at Mineral Optics Laboratory for preparing the specimens.

7. REFERENCES

Caulk, R. A., Ghazanfari, E., Perdrial, J. N., & Perdrial, N. (2016). Experimental investigation of fracture aperture and permeability change within Enhanced Geothermal Systems. *Geothermics*, *62*, 12-21.

Cladouhos, T.T., Petty, S., Swyer, M.W., Uddenberg, M.E., Grasso, K., Nordin, Y., (2016). Results from newberry volcano EGS demonstration, 2010–2014. *Geothermics*, 63, 44–61.

Faoro, I., Elsworth, D., & Candela, T. (2016). Evolution of the transport properties of fractures subject to thermally and mechanically activated mineral alteration and redistribution. *Geofluids*, *16*(3), 396-407.

Frash, L. P., Gutierrez, M., & Hampton, J. (2014). True-triaxial apparatus for simulation of hydraulically fractured multi-borehole hot dry rock reservoirs. *International Journal of Rock Mechanics and Mining Sciences*, *70*, 496-506.

Ghassemi, A. (2012). A review of some rock mechanics issues in geothermal reservoir development. *Geotechnical and Geological Engineering*, *30*(3), 647-664.

Ghassemi, A., & Kumar, G. S. (2007). Changes in fracture aperture and fluid pressure due to thermal stress and silica dissolution/precipitation induced by heat extraction from subsurface rocks. *Geothermics*, *36*(2), 115-140.

Kamali-Asl, A., Ghazanfari, E., Perdrial, N., & Bredice, N. (2018). Experimental study of fracture response in granite specimens subjected to hydrothermal conditions relevant for enhanced geothermal systems. *Geothermics*, *72*, 205-224.

Kamali-Asl, A., Kc, B., Foroutan, M., Ghazanfari, E., Cladouhos, T. T., & Stevens, M. (2019). Stress-strain response and seismic signature analysis of phyllite reservoir rocks from Blue Mountain geothermal field. *Geothermics*, *77*, 204-223.

Majer, E. L., Baria, R., Stark, M., Oates, S., Bommer, J., Smith, B., & Asanuma, H. (2007). Induced seismicity associated with enhanced geothermal systems. *Geothermics*, *36*(3), 185-222.

McClure, M. W., & Horne, R. N. (2014). An investigation of stimulation mechanisms in Enhanced Geothermal Systems. *International Journal of Rock Mechanics and Mining Sciences*, *72*, 242-260.

Oldenburg, C. M., Dobson, P. F., Wu, Y., Cook, P. J., Kneafsey, T. J., Nakagawa, S., ... & Rutqvist, J. (2017, February). Hydraulic fracturing experiments at 1500 m depth in a deep mine: Highlights from the kISMET project. *In Proceedings, 42nd Workshop on Geothermal Reservoir Engineering, Stanford University*.

Polak, A., Elsworth, D., Yasuhara, H., Grader, A. S., & Halleck, P. M. (2003). Permeability reduction of a natural fracture under net dissolution by hydrothermal fluids. *Geophysical Research Letters*, *30*(20).

Riahi, A., & Damjanac, B. (2013, February). Numerical study of hydro-shearing in geothermal reservoirs with a pre-existing discrete fracture network. In *Proceedings of the 38th Workshop on Geothermal Reservoir Engineering, Stanford, CA* (pp. 11-13).

Swyer, M., Uddenberg, M., Nordin, Y., Cladouhos, T. and Petty, S. (2016). New Injection Strategies at Blue Mountain, Nevada Through Tracer Test Analysis, Injection-Production Correlation, and an Improved Conceptual Model. *Forty-first Workshop on Geothermal Reservoir Engineering,* Stanford University, Stanford, California, February 22-24, 2016. SGP-TR-209.

Taron, J., & Elsworth, D. (2009). Thermal–hydrologic–mechanical–chemical processes in the evolution of engineered geothermal reservoirs. *International Journal of Rock Mechanics and Mining Sciences*, *46*(5), 855-864.

Tester, J. W., Anderson, B. J., Batchelor, A. S., Blackwell, D. D., DiPippo, R., Drake, E., ... & Petty, S. (2006). The future of geothermal energy: Impact of enhanced geothermal systems (EGS) on the United States in the 21st century. *Massachusetts Institute of Technology*, *209*.

Vogler, D., Amann, F., Bayer, P., & Elsworth, D. (2016). Permeability evolution in natural fractures subject to cyclic loading and gouge formation. *Rock Mechanics and Rock Engineering*, 49(9), 3463-3479.

Watanabe, N., Egawa, M., Sakaguchi, K., Ishibashi, T., & Tsuchiya, N. (2017). Hydraulic fracturing and permeability enhancement in granite from subcritical/brittle to supercritical/ductile conditions. *Geophysical Research Letters, 44*(11), 5468-5475.

Witherspoon, P. A., Wang, J. S., Iwai, K., & Gale, J. E. (1980). Validity of cubic law for fluid flow in a deformable rock fracture. *Water resources research*, *16*(6), 1016-1024.

Yasuhara, H., & Elsworth, D. (2008). Compaction of a rock fracture moderated by competing roles of stress corrosion and pressure solution. *Pure and Applied Geophysics*, 165(7), 1289-1306.

Yasuhara, H., Elsworth, D., & Polak, A. (2004). Evolution of permeability in a natural fracture: Significant role of pressure solution. *Journal of Geophysical Research: Solid Earth*, *109*(B3).

Yasuhara, H., Kinoshita, N., Ohfuji, H., Lee, D. S., Nakashima, S., & Kishida, K. (2011). Temporal alteration of fracture permeability in granite under hydrothermal conditions and its interpretation by coupled chemo-mechanical model. *Applied Geochemistry*, *26*(12), 2074-2088.

Yu, Y., Zhang, J., & Zhang, J. (2009). A modified Brazilian disk tension test. *International Journal of Rock Mechanics and Mining Sciences*, 2(46), 421-425.